NACA RM L55B16

NACA

RESEARCH MEMORANDUM

TRANSONIC FLUTTER INVESTIGATION OF A FIGHTER-AIRPLANE WING MODEL AND COMPARISON WITH A SYSTEMATIC PLAN-FORM SERIES

By Norman S. Land and Frank T. Abbott, Jr.

Langley Aeronautical Laboratory
Langley Field, Va.

NATIONAL ADVISORY COMMITTEE
FOR AERONAUTICS

WASHINGTON
October 7, 1955
Declassified October 28, 1960

NACA RM L55B16

NATIONAL ADVISORY COMMITTEE FOR AERONAUTICS

RESEARCH MEMORANDUM

TRANSONIC FLUTTER INVESTIGATION OF A FIGHTER-AIRPLANE WING MODEL AND COMPARISON WITH A SYSTEMATIC PLAN-FORM SERIES

By Norman S. Land and Frank T. Abbott, Jr.

SUMMARY

An investigation was made of the transonic flutter characteristics at zero lift of a model of a wing for a new fighter airplane. The results showed that the flutter characteristics of the fighter wing model were similar to those of a comparable systematic plan-form series of models partially reported in NACA RM L53G10a. It was also found that a change in airfoil section from one with a slight leading-edge droop and chord-extension to a symmetrical NACA section did not affect the flutter characteristics.

INTRODUCTION

The National Advisory Committee for Aeronautics was requested to determine the transonic flutter boundaries of the wing and tail of a new fighter airplane by means of model tests in the Langley transonic blow-down tunnel. This report presents the results of one of these investigations, that of determining the zero-lift flutter characteristics of a model of the airplane wing over a range of Mach numbers from 0.85 to 1.34. The range of Reynolds numbers was generally between 2.0×10^6 and 6.5×10^6 (based on streamwise root chord), and the range of density ratios μ was from 40 to 120.

Although the plan form of this wing was covered in the range of the systematic series of wing plan forms reported in reference 1, two possibly important differences in geometry were present in this wing: thickness-ratio taper and leading-edge camber or droop. Tests of this specific wing were, therefore, felt desirable in order to gain some appreciation of the importance of these two differences. The wing tested had an aspect ratio of 4, a taper ratio of 0.5, 35° of sweepback, 2.5° of negative dihedral, airfoil sections tapering in thickness from 6 percent at the root to 4 percent at the tip, and a rounded tip. The

airplane wing has an NACA symmetrical airfoil section modified to incorporate a slight leading-edge droop and chord-extension. Models with these sections and with unmodified NACA symmetrical sections were tested.

The results are presented as the ratio of experimental flutter speed to a calculated subsonic flutter speed based on a well-known method.

SYMBOLS

A	aspect ratio including body intercept
a	distance in wing half-chords from midchord to elastic-axis position, measured positive rearward
b	half-chord perpendicular to quarter-chord line, ft
b_r	half-chord perpendicular to quarter-chord line at intersection of quarter-chord line and fuselage, ft
EI	wing bending stiffness, lb-in.^{2}
GJ	wing torsional stiffness, lb-in.^{2}
g	structural-damping coefficient
I_α	polar moment of inertia of wing section about elastic axis, slug-ft^2/ft
k	reduced-frequency parameter, $\frac{\omega b}{V}$
l	length of wing panel along quarter-chord line from intersection of quarter-chord line with edge of fuselage to intersection with theoretical tip, ft
M	Mach number
m	mass of wing per unit length along quarter-chord line, slugs/ft
q	dynamic pressure, lb/sq in.
r_α	nondimensional radius of gyration of wing section about elastic axis, $\left(I_\alpha / mb^2\right)^{1/2}$

V	stream velocity, ft/sec
V_e/V_R	flutter-speed ratio
x_α	distance in half-chords from wing section elastic-axis position to wing section center-of-gravity position measured perpendicular to quarter-chord line, measured positive rearward
η	nondimensional coordinate along quarter-chord line, fraction of length l
μ	ratio of mass of wing to mass of cylinder of air of diameter equal to chord of wing, both taken for equal length along quarter-chord line, $m/\pi\rho b^2$
Λ	angle of sweepback of quarter-chord line, deg
ρ	air density, slugs/cu ft
ω	angular frequency of vibration, radians/sec

Subscripts:

α	uncoupled torsion mode
e	experimental values at start of flutter
R	calculated values

MODELS

The models tested had an aspect ratio (including body intercept) of 4, a taper ratio of 0.5, a sweep angle of 35° of the quarter chord, and rounded tips. Each of the models had 2.5° of negative dihedral. The airfoil sections(streamwise) of all models tapered from approximately 6 percent in thickness at the root to approximately 4 percent at the tip. Models employing two different airfoil sections were tested. One model, designated model 9, had an NACA 65A006 airfoil section at the root and an NACA 65A004 section at the tip. Two other models (models 7A and 14) had airfoil sections modified from the above NACA 65A-sections to incorporate a slight leading-edge droop and chord-extension. The pertinent dimensions of the models are given in figure 1.

Model 7A was made from solid mahogany with a sprayed, exterior coating of a phenolic-base material. This coating, which was approximately 0.006 inch thick, was employed in order to stiffen the model. Models 9 and 14 were made of laminated wood with the laminations running spanwise. The laminations were alternately mahogany and a compressed, plastic impregnated wood. Each lamination was approximately 1/8 inch wide.

The bending and torsional stiffnesses given in table I were determined from the load-deflection relationships at several stations, the bending or torsion loads being applied near the tip of the wing which was mounted as a cantilever. The deflections were measured with the aid of an optical system. A light source and telescope projected an image of the cross hairs of the telescope in a direction perpendicular to the chord plane of the wing. At each spanwise station, a 1/8-inch-square plane mirror was mounted on the surface of the wing. The reflected image of the cross hairs was projected on a scale a sufficient distance away to result in adequate deflection of the image for small angular deflections of the mirror.

In order to determine the natural frequencies of vibration, the model was mounted as a cantilever, as in the tunnel tests, and excited at various frequencies. Excitation was accomplished by means of an electrodynamic vibrator driven by a variable-frequency audio oscillator. The vibrator was applied at various points along a chord line at approximately 0.2 panel span. Node lines were found by sprinkling table salt on the upper surface of the wing and observing the lines along which the grains remained stationary. The resulting data are given in figures 2 to 4. No measurements of mode shapes were made.

The chordwise location of the elastic axis of each wing was determined at a number of spanwise stations by applying a concentrated bending load at several positions along the chord line. The chordwise position of the load which resulted in only bending deflection located a point on the elastic axis. Deflections were observed with the aid of the optical system previously described. Location of the elastic axis for each wing is given in table I.

Subsequent to the tests, one wing panel of each model was sawed into segments perpendicular to the quarter-chord line. With these segments, the mass per unit length and center-of-gravity location were determined. Each segment was swung on a torsion pendulum to determine its moment of inertia about the elastic axis. Data thus obtained on locations of the center of gravity, the mass, and the moment of inertia are given in table I.

The structural-damping coefficients in bending were determined from a study of the decrement of free bending vibrations. An average value

of all three models was 0.018. Some variation in these determinations existed for each model as well as between models but the magnitude of the variations was such as to cause only a 1- or 2-percent variation in calculated flutter speed.

APPARATUS AND TESTS

Wind Tunnel

The tests described in this report were conducted in the Langley transonic blowdown tunnel. This tunnel and its initial use in a flutter investigation are described in reference 2 which compares transonic flutter data from several sources. The value of the Langley transonic blowdown tunnel for a flutter investigation lies in the fact that the Mach number can be held constant (by operating choked) while the density is gradually increased until flutter occurs. Since the flutter velocity is dependent on the air density and the Mach number, one model may be fluttered at several Mach numbers by using different sizes of the downstream orifice plates which control the Mach number at which the orifice chokes. An additional feature of the tunnel is that the air-supply valves may be closed rapidly and, therefore, prevent the model from fluttering to destruction.

Model Support

The model was supported as shown in figure 5 by a 3-inch-diameter steel fuselage, the chord plane of the wing intersecting the fuselage near its center line. This fuselage was cylindrical in form and was alined with the center of the tunnel. It extended upstream into the settling chamber where the air velocity is low. Because the fuselage nose was in a low-velocity region and because there was no fuselage support in the test section ahead of the model, no shock waves were generated by the fuselage which could reflect from the tunnel walls back on the model.

Instrumentation

All the data taken were recorded as time histories by a recording oscillograph. The signals from the various pickups were fed to the oscillograph elements through appropriate amplifiers. Motions of the wing panels of the model were recorded through the use of strain gages mounted near the root of each panel. Two sets of gages on each panel were oriented so that one set was sensitive primarily to bending deflections and the other was sensitive primarily to torsional deflections of the panel.

In addition to the instrumentation used for recording data, some instrumentation was used which was designed to aid in conducting the tests. The model could be observed directly by the test crew with the use of an optical system which projected an image of the wing on a ground-glass screen in the test house. In the early phases of the test, some high-speed motion pictures (approximately 1,500 frames per second) were taken during flutter. These were studied to determine qualitatively whether the lowest bending and torsion modes would approximate the elastic curves of the wing during flutter.

Because of the difficulty in distinguishing between buffeting, intermittent flutter, and steady flutter when directly viewing the model, an additional observation method was employed. In this system, the amplified signals from the bending and torsion strain gages were applied to two cathode-ray oscilloscopes, one oscilloscope for each wing panel. The bending signals were applied to the vertical axes of the oscilloscopes and the torsion signals to the horizontal axes. This method of presentation gave a clearly recognizable pattern for each type of vibration encountered by the model. Buffeting, or forced oscillations, of the model resulted in a random, jumbled pattern on the oscilloscopes. Steady flutter resulted in a simple Lissajous figure inasmuch as both bending and torsional oscillations occur at the same frequency during flutter. Intermittent flutter therefore made a pattern changing from the random to the simple.

Method of Testing

Prior to making flutter observations, the model was adjusted to zero lift. This was done by making a low-speed run and observing the model on the viewing screen. Adjustment of the angle of attack of the model was made until no bending deflection of the wing tips could be observed.

Each run was made by continually opening the air-supply valves which continually increased the dynamic pressure until steady flutter was observed. Steady flutter was allowed to continue for only a second or two; then the air-supply valves were closed. These runs were made with various tunnel orifice plates so that the available Mach number range was covered. As a check on the structural integrity of the model, an oscillograph record of the free bending vibrations of each wing panel was made before every run. Later examination of these records showed whether flutter had caused structural damage to the model as evidenced by any changes in natural frequency or damping.

COMPUTATIONS

Reference flutter speeds V_R and frequencies ω_R were computed for each model and are given in table II for each experimental flutter point. The use of reference flutter speed as a means of reducing experimental flutter data to a comparable basis has been discussed in references 1 and 3, and the methods of computation outlined in these reports were followed in the present investigation.

The computations were based on two-dimensional incompressible-flow aerodynamic coefficients, and the terms involving the spanwise derivative of the velocity potential were omitted.

The effect of wing taper was brought into the aerodynamic terms by weighting the reduced frequency k according to the chord variation and by representing the Theodorsen functions $F(k)$ and $G(k)$ by a linear variation between their root and tip values. As was mentioned in reference 1, representing the Theodorsen functions in this manner was a convenience in setting up the computations for automatic, punchcard computing equipment; comparative checks by manual computing methods showed excellent agreement.

The effective length of each wing panel is defined in the calculations as the length of the quarter-chord line between the tip and the intersection with the fuselage (fig. 1). Various physical parameters given in table II are defined in relation to this line or perpendicular to it as applicable.

The two lowest uncoupled mode shapes of a uniform cantilever beam given in reference 4 were used to approximate the flutter modes as was done in reference 1. Frequencies used in the calculations were measured as described in a preceding section. Although these corresponded to coupled modes of vibration, application of the method of reference 3 showed that the values used were close to those of the uncoupled modes.

Values of the flutter-speed parameter $V_R/b\omega_\alpha$ were obtained from the solution of the flutter-stability determinant as a function of the structural damping for given values of the air density. The assumption was made in these calculations that the structural damping in bending was equal to that in torsion. Values of the reference flutter speed V_R were then obtained by using the measured structural damping in bending for each wing, together with the appropriate air density.

RESULTS AND DISCUSSION

The experimental data that were obtained are given in table II. Included in this table are the corresponding calculated reference flutter speeds and frequencies.

Visual observations made during these tests and the tests of reference 1 indicated that flutter did not always begin suddenly and violently. Subsequent examination of the test records verified this observation. Typical samples from the oscillograph records of bending and torsion strain-gage output for one wing panel illustrate this point in figure 6, although amplitudes of oscillations in part (a) should not be compared with those in parts (b) and (c) because of differences in amplification. At subsonic Mach numbers, flutter tended to start with explosive violence and with little or no previous warning as shown in figure 6(a). At the higher supersonic Mach numbers, within the range of these tests, a region of low damping was encountered before sustained flutter occurred. This region of low damping was characterized by bursts of relatively low-amplitude, short-duration flutter as shown in figure 6(b). With further increase in speed or air density, the damping decreased slowly, as evidenced by an increasing number of flutter bursts, until finally a sustained large-amplitude flutter condition was reached as shown in figure 6(c).

Some appreciation of the change in damping as sustained flutter is approached may be gained from the typical examples shown in figure 7. This figure shows the frequencies of bending and torsional oscillations (indicated by the strain-gage records) as the dynamic pressure was increased from zero to that for both subsonic and supersonic flutter. These data can be considered as crude frequency spectra of the bending and torsional oscillations as flutter is approached. At zero dynamic pressure, of course, no oscillations were actually observed, but any disturbance of the model would result in oscillations at the lowest natural frequencies in bending and torsion. At low values of dynamic pressure, airstream disturbances resulted in oscillations at frequencies near these still-air natural frequencies. As the dynamic pressure increased, the frequencies of oscillation in bending and torsion approached each other and when flutter occurred they were equal. As illustrated in figure 7(a) for subsonic flutter, the two frequencies approached each other rapidly and the spectra of the frequencies were narrow. However, an approach to flutter at a supersonic Mach number, as illustrated in figure 7(b), was characterized by rather wide frequency spectra and a region of overlapping of the extremes of the bending and torsional spectra. It is this region where low damping was indicated by intermittent flutter. Steady flutter is indicated in figure 7 by the predominant bending and torsional frequencies being equal. All the data taken were analyzed in this fashion as an aid in determining a boundary of intermittent flutter as well as

steady flutter. The extent of the region of low damping as a function of Mach number is shown for a typical model in figure 8. Since free-air conditions may be much more steady than those of the tunnel, intermittent flutter in the region of low damping may not occur in flight as was observed during the model tests. The limited extent and detail of free-flight-flutter information, however, precludes comparisons of behavior in the low-damping region between wind-tunnel and flight tests.

The ratio of the experimental sustained flutter speeds to the reference flutter speed for the three models is shown in figure 9. For comparison, curves for wings with 30° and 45° of sweep are also given in figure 9. These curves are data (unpublished) from a continuation of the systematic series reported in reference 1. These latter wings had symmetrical airfoil sections of 4-percent thickness, an aspect ratio of 4, a taper ratio of 0.6, square-tip plan forms, and no dihedral. It can be seen that the flutter-speed ratios of the practical wings of the present investigation with 35° of sweep fall in between those of the 30° and 45° swept wings over the range of Mach numbers from about 0.95 to 1.25. At a Mach number of about 0.9, the fighter-wing data show a dip in the flutter-speed ratio. This same tendency was shown in the data of reference 5. At Mach numbers from 1.2 to 1.34, there seems to be a definite tendency for the flutter-speed ratio to level off, whereas the curves of the 30° and 45° swept wings show a continual rise in flutter-speed ratio as the Mach number is increased. The reason for the difference is not known. Presumably the major causes are location of the center of pressure and the phase relation between air forces and moment.

The data of figure 9 also show that the flutter-speed ratio was not affected, within the accuracy of the data, by slightly drooping the leading edge of the airfoil section.

CONCLUSIONS

The results of flutter tests at zero lift of a model of the wing of a new fighter airplane and comparison with those of a somewhat idealized systematic plan-form investigation indicate the following conclusions:

1. Tests of a model of the wing for a high-speed fighter airplane showed that its variation of flutter-speed ratio with Mach number was similar to those of the systematic series of wing models having comparable plan forms. It was of particular interest that the same flutter characteristics were exhibited by a model which had airfoil sections incorporating a slight leading-edge droop and chord-extension and a model which had a similar plan form but had symmetrical NACA airfoil sections.

2. The calculated flutter speeds agreed with the experimental flutter speeds at a Mach number of 0.9.

3. It was observed that at subsonic Mach numbers flutter started with little or no warning; but, as the Mach number was increased to supersonic values, a widening region of intermittent flutter preceded sustained flutter.

Langley Aeronautical Laboratory,
National Advisory Committee for Aeronautics,
Langley Field, Va., February 7, 1955.

REFERENCES

1. Jones, George W., Jr., and DuBose, Hugh C.: Investigation of Wing Flutter at Transonic Speeds for Six Systematically Varied Wing Plan Forms. NACA RM L53G10a, 1953.

2. Bursnall, William J.: Initial Flutter Tests in the Langley Transonic Blowdown Tunnel and Comparisons With Free-Flight Flutter Results. NACA RM L52K14, 1953.

3. Barmby, J. G., Cunningham, H. J., and Garrick, I. E.: Study of Effects of Sweep on the Flutter of Cantilever Wings. NACA Rep. 1014, 1951. (Supersedes NACA TN 2121.)

4. Anderson, Roger A., and Houbolt, John C.: Determination of Coupled and Uncoupled Modes and Frequencies of Natural Vibration of Swept and Unswept Wings From Uniform Cantilever Modes. NACA TN 1747, 1948.

5. Pratt, George L.: Experimental Flutter Investigation of a Thin Unswept Wing at Transonic Speeds. NACA RM L55A18, 1955.

TABLE I.- MODEL PARAMETERS AT SPANWISE STATIONS

[All values at η = 0.05, 0.15, and 0.25 are extrapolated]

η	x_α	a	r_α^2	m, slugs/ft	b/b_r	EI, lb-in.^{2}	GJ, lb-in.^{2}
Model 7A							
0.05	-0.347	0.185	0.262	0.00745	0.994	-----	-----
.15	-.304	.155	.266	.00660	.946	-----	-----
.25	-.260	.125	.278	.00575	.898	-----	-----
.35	-.215	.095	.291	.00495	.850	2,320	1,680
.45	-.172	.065	.296	.00435	.802	1,690	1,120
.55	-.128	.034	.292	.00382	.755	1,300	770
.65	-.085	.004	.280	.00340	.710	1,000	560
.75	-.040	-.027	.273	.00300	.661	840	430
.85	.002	-.057	.268	.00266	.616	720	330
.95	.045	-.087	.265	.00232	.569	610	250
Model 9							
0.05	-0.0640	-0.052	0.237	0.00942	0.983	-----	---
.15	-.0688	-.044	.238	.00822	.936	-----	---
.25	-.0735	-.033	.240	.00717	.890	-----	---
.35	-.0793	-.020	.245	.00616	.843	2,700	---
.45	-.0865	-.006	.255	.00537	.796	1,950	860
.55	-.0931	.008	.262	.00480	.750	1,520	590
.65	-.1006	.025	.268	.00434	.703	1,160	460
.75	-.1116	.044	.268	.00396	.656	840	370
.85	-.1224	.066	.267	.00363	.609	560	295
.95	-.1352	.092	.260	.00333	.563	390	230
Model 14							
0.05	0.1352	-0.1976	0.2127	0.01297	0.995	-----	-----
.15	.1158	-.1786	.2228	.01087	.949	-----	-----
.25	.0933	-.1550	.2336	.00898	.902	-----	-----
.35	.0690	-.1312	.2406	.00758	.856	-----	-----
.45	.0407	-.1027	.2462	.00670	.810	2,420	1,280
.55	.0116	-.0716	.2520	.00588	.764	1,810	800
.65	-.0233	-.0377	.2640	.00514	.718	1,330	590
.75	-.0631	.0044	.2762	.00442	.671	970	440
.85	-.1056	.0496	.2937	.00373	.625	705	340
.95	-.1573	.1003	.3009	.00308	.579	530	250

TABLE II.- EXPERIMENTAL AND ANALYTICAL RESULTS

ρ_e, slugs/cu ft	q_e, lb/sq in.	ω_e, radians/sec	V_e, ft/sec	M_e	ω_R, radians/sec	V_R, ft/sec	V_e/V_R	ω_e/ω_R
Model 7A								
0.00240	7.55	1,344	968	0.926	1,586	987	0.981	0.847
.00280	8.64	1,350	945	.910	1,618	923	1.024	.834
.00280	7.51	1,382	891	.864	1,618	923	.965	.854
.00274	8.07	1,350	922	.911	1,614	932	.989	.836
.00310	9.13	1,340	927	.933	1,640	886	1.047	.817
.00440	21.33	1,947	1,178	1.222	1,709	773	1.524	1.139
.00459	16.86	1,921	1,038	1.082	1,717	758	1.356	1.123
Model 9								
0.00290	8.68	1,170	928	.873	1,365	891	1.042	.857
.00316	9.32	1,257	922	.885	1,380	862	1.069	.911
.00348	13.71	1,571	1,064	1.051	1,397	830	1.282	1.125
.00396	18.05	1,571	1,144	1.159	1,418	790	1.448	1.108
.00404	19.82	1,571	1,189	1.219	1,421	784	1.516	1.105
.00406	20.00	1,559	1,190	1.227	1,422	782	1.522	1.096
.00406	16.02	1,596	1,065	1.072	1,422	782	1.362	1.122
.00416	10.25	1,258	841	.823	1,426	774	1.087	.882
.00418	17.10	1,520	1,085	1.135	1,427	773	1.404	1.065
.00429	19.38	1,595	1,141	1.164	1,432	765	1.492	1.114
.00436	22.00	1,595	1,204	1.343	1,434	760	1.584	1.112
.00442	15.23	1,558	996	1.039	1,437	755	1.319	1.084
.00458	18.28	1,571	1,072	1.128	1,443	744	1.441	1.089
.00460	22.15	1,583	1,177	1.232	1,443	742	1.586	1.097
.00484	23.49	1,621	1,182	1.331	1,453	725	1.630	1.116
Model 14								
0.00381	13.56	1,570	1,012	.988	1,527	815	1.242	1.030
.00394	15.88	1,570	1,077	1.069	1,534	803	1.341	1.023
.00446	19.26	1,570	1,115	1.120	1,558	755	1.477	1.010
.00447	20.01	1,510	1,135	1.121	1,559	761	1.492	.970
.00470	12.22	1,440	864	.833	1,569	746	1.158	.919
.00470	21.21	1,570	1,139	1.162	1,569	746	1.520	1.000

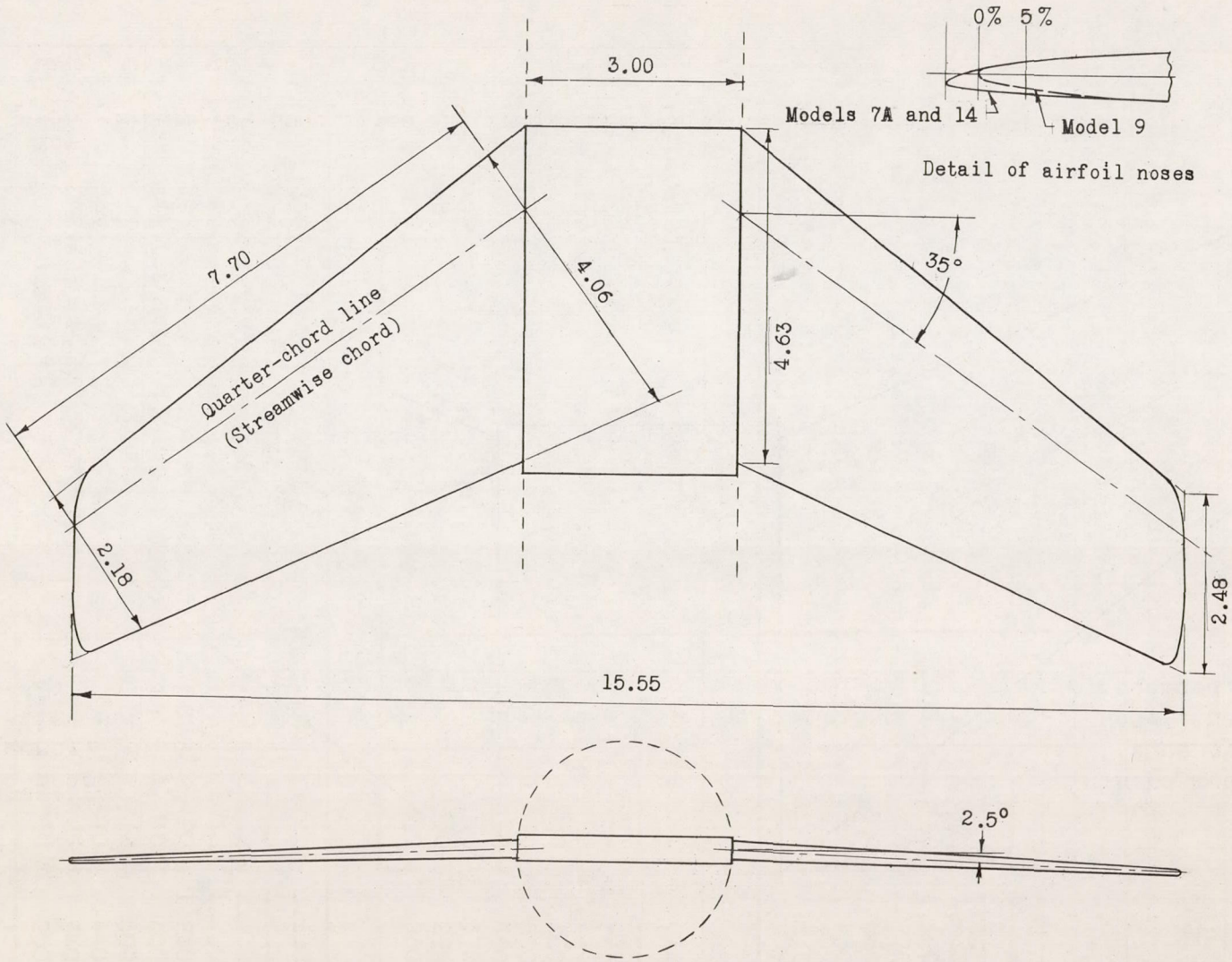

Figure 1.- Wing model for flutter tests. Dimensions in inches.

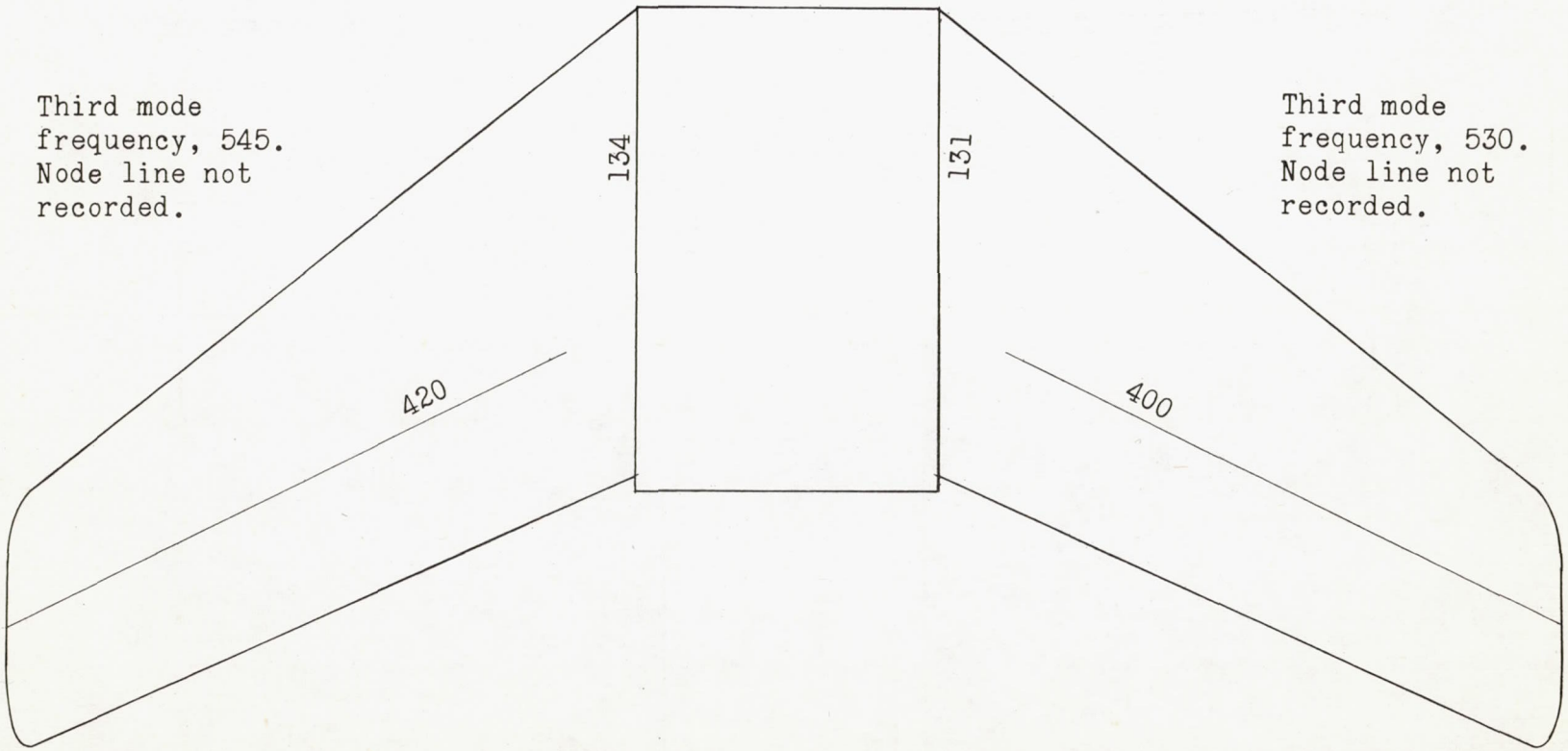

Figure 2.- Node lines and frequencies in cycles per second. Model 7A.

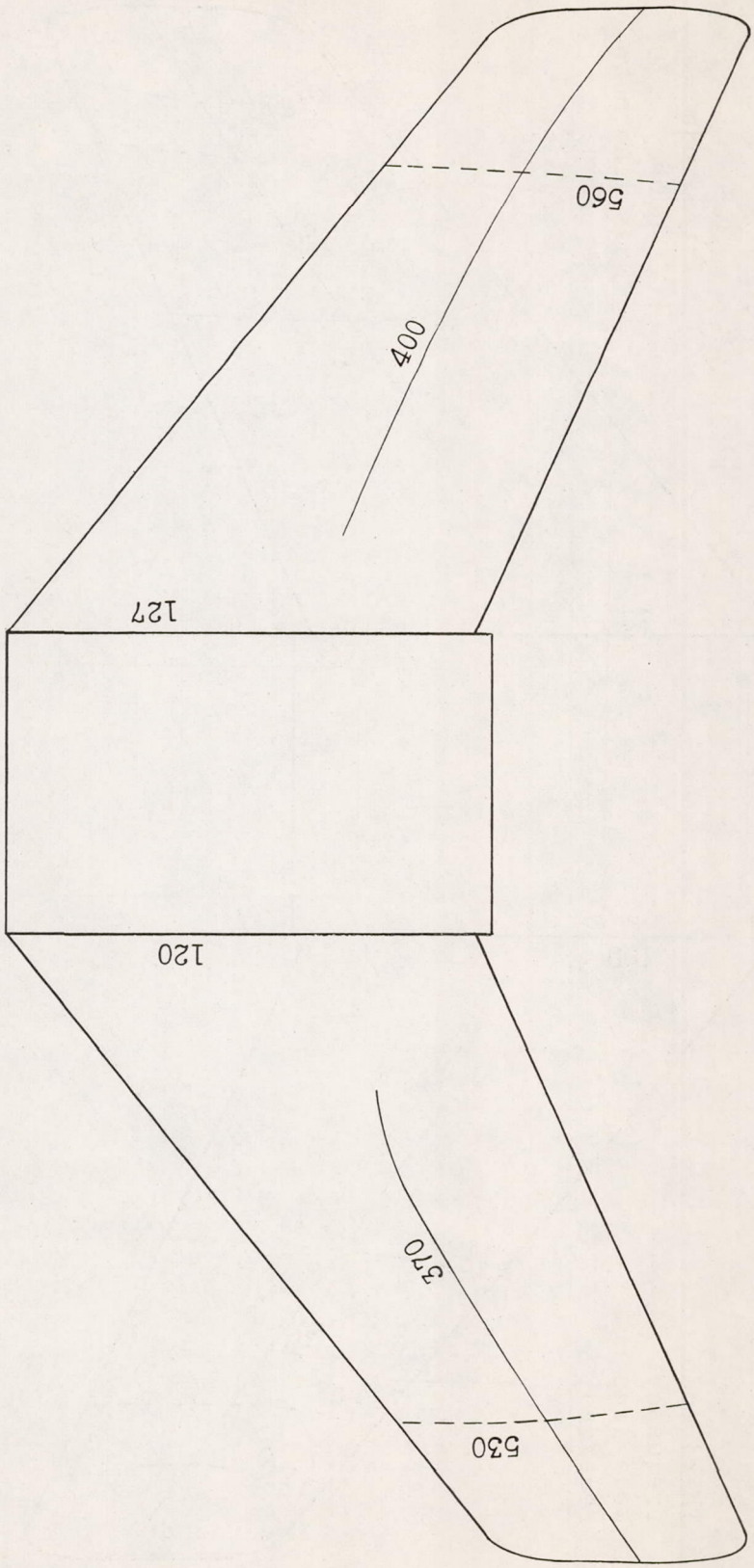

Figure 3.- Node lines and frequencies in cycles per second. Model 9.

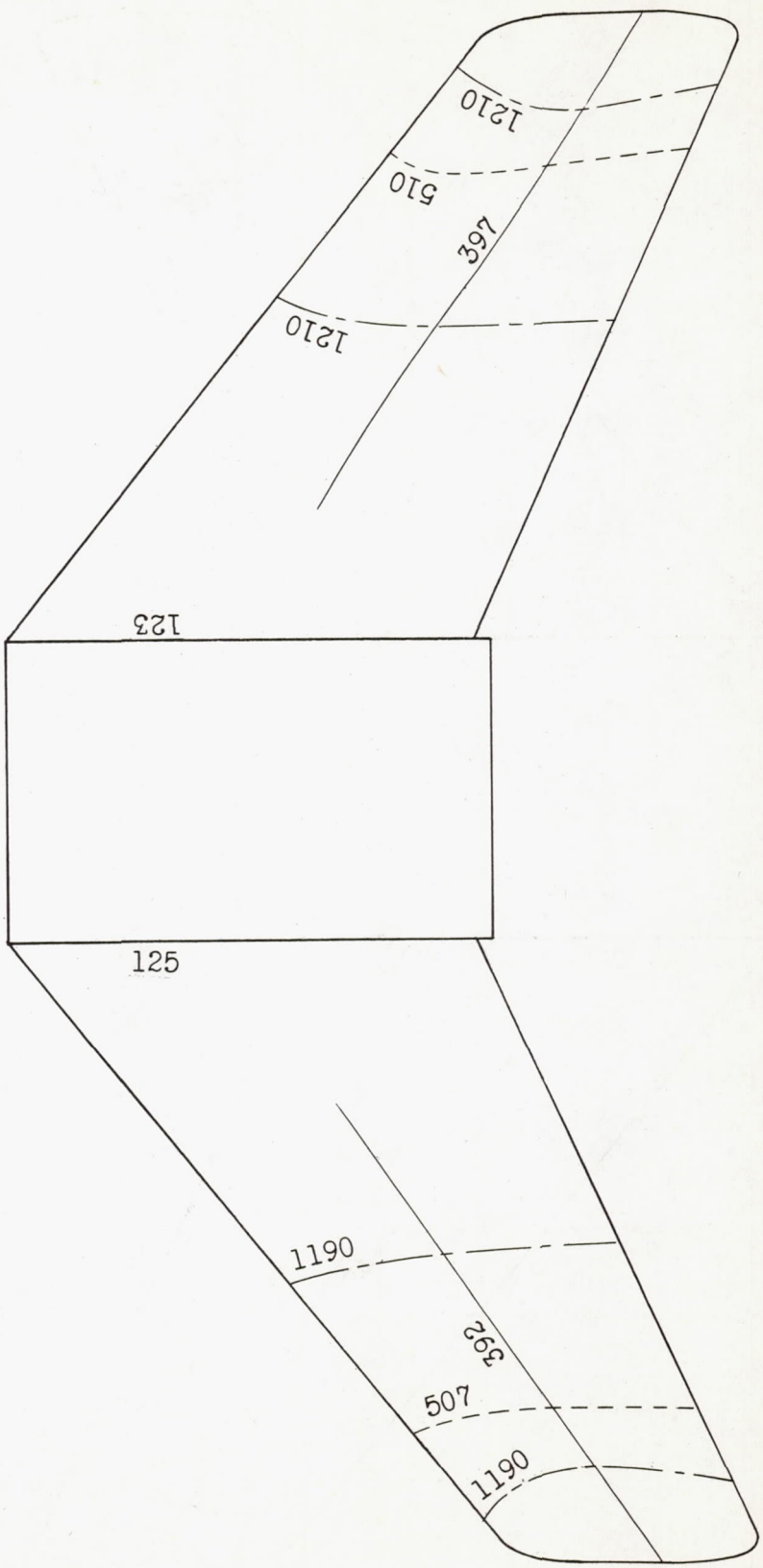

Figure 4.- Node lines and frequencies in cycles per second. Model 14.

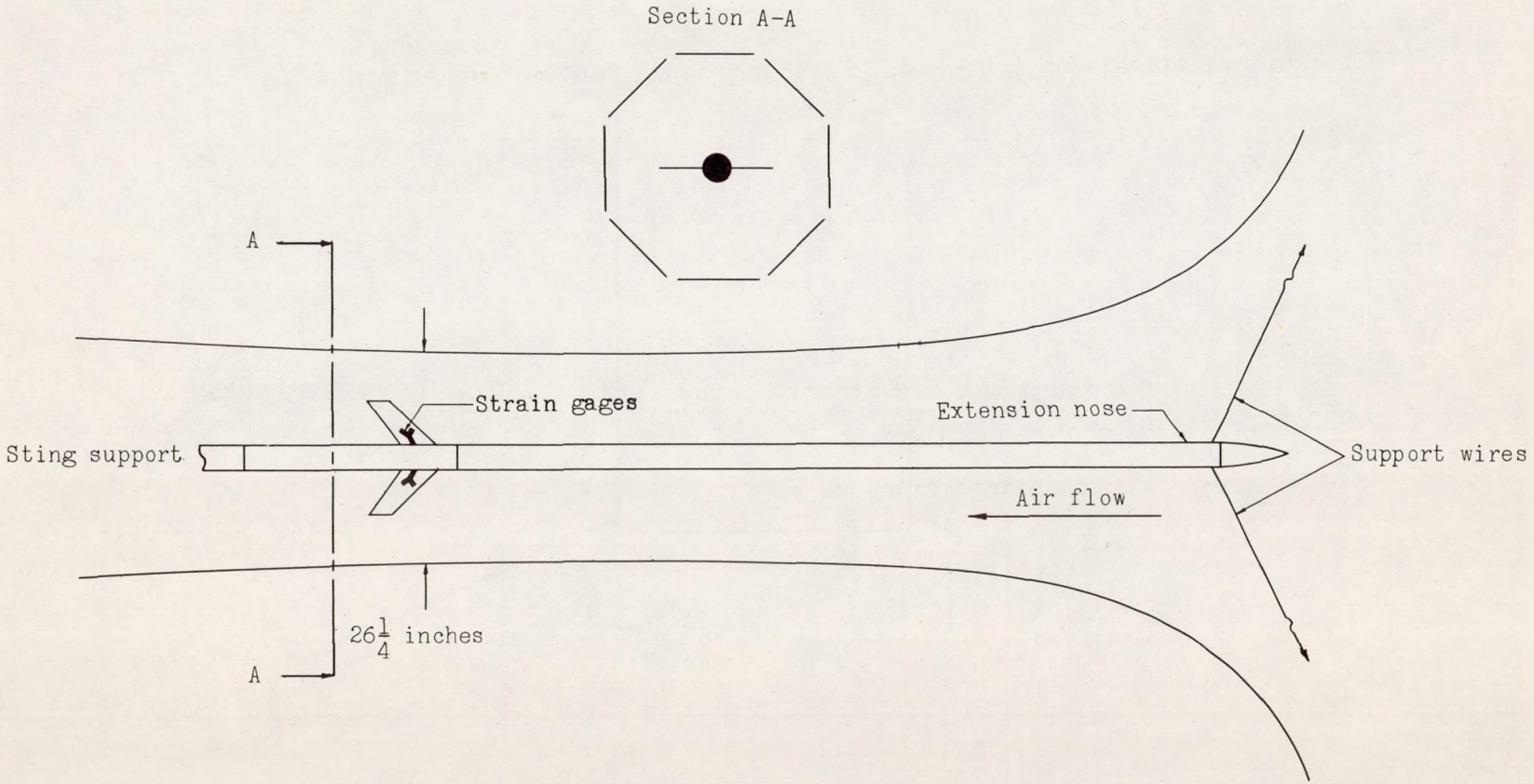

Figure 5.- Plan view of Langley transonic blowdown tunnel with flutter model installed.

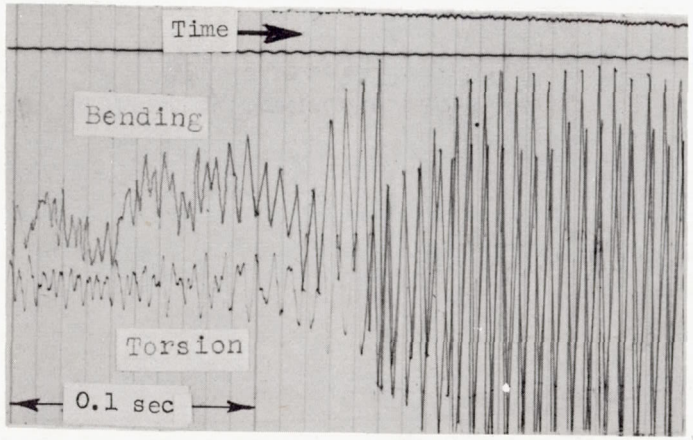

(a) Typical start of subsonic flutter.

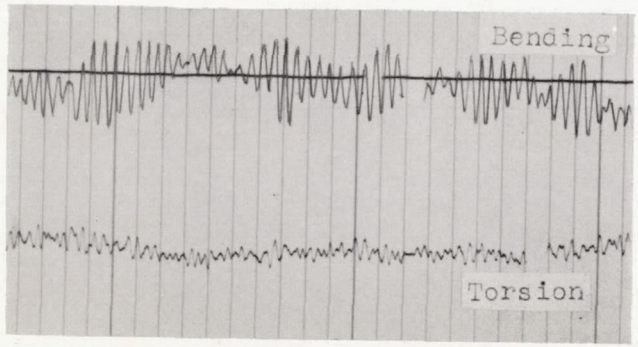

(b) Region of low damping preceding supersonic flutter.

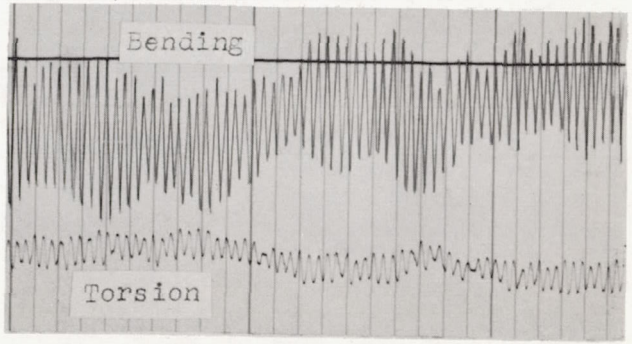

(c) Sustained supersonic flutter.

Figure 6.- Typical sections of oscillograph records showing bending and torsional oscillations before and during flutter at subsonic and supersonic speeds.

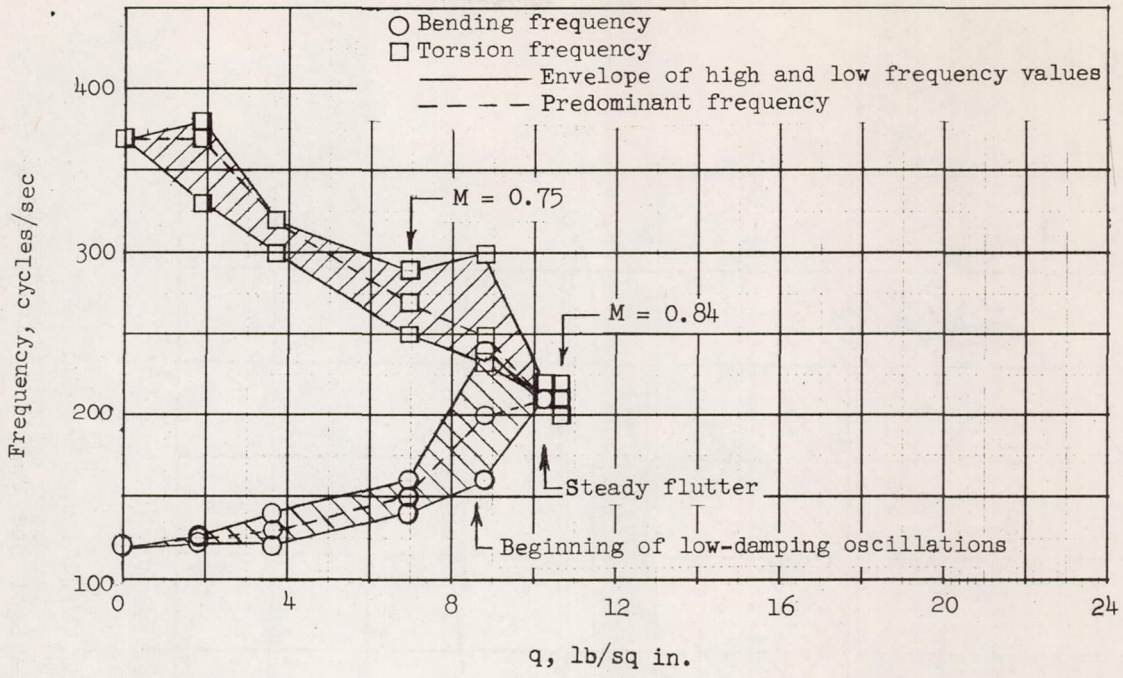

(a) Subsonic flutter.

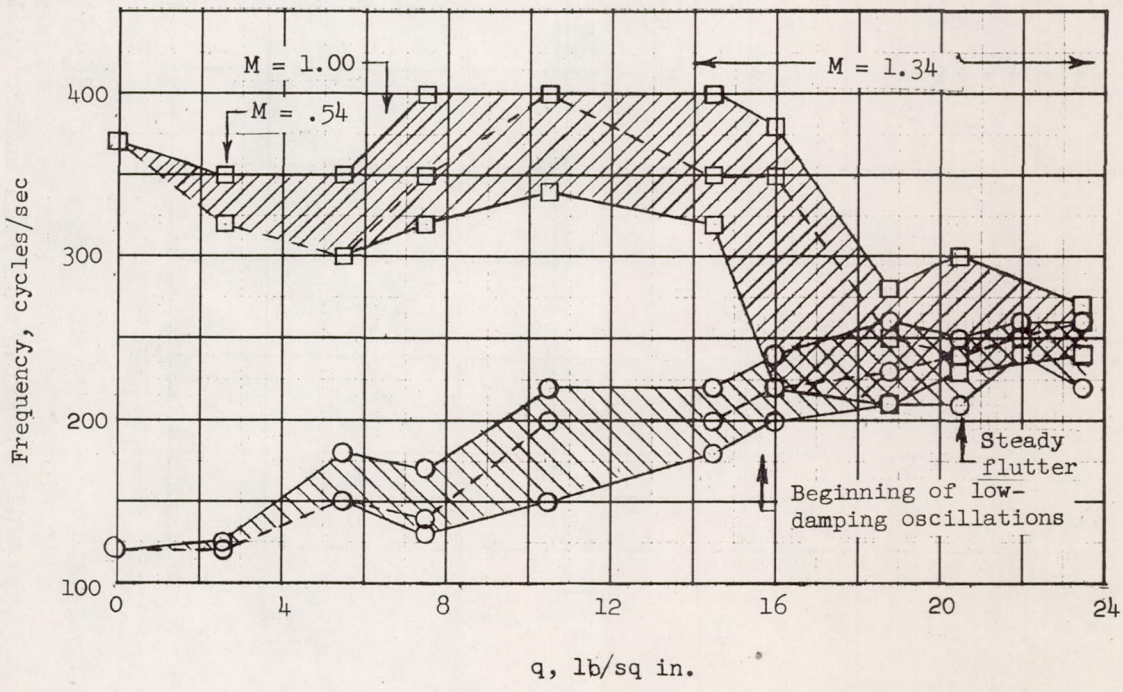

(b) Supersonic flutter.

Figure 7.- Variation of bending and torsion frequencies with dynamic pressure during a test run.

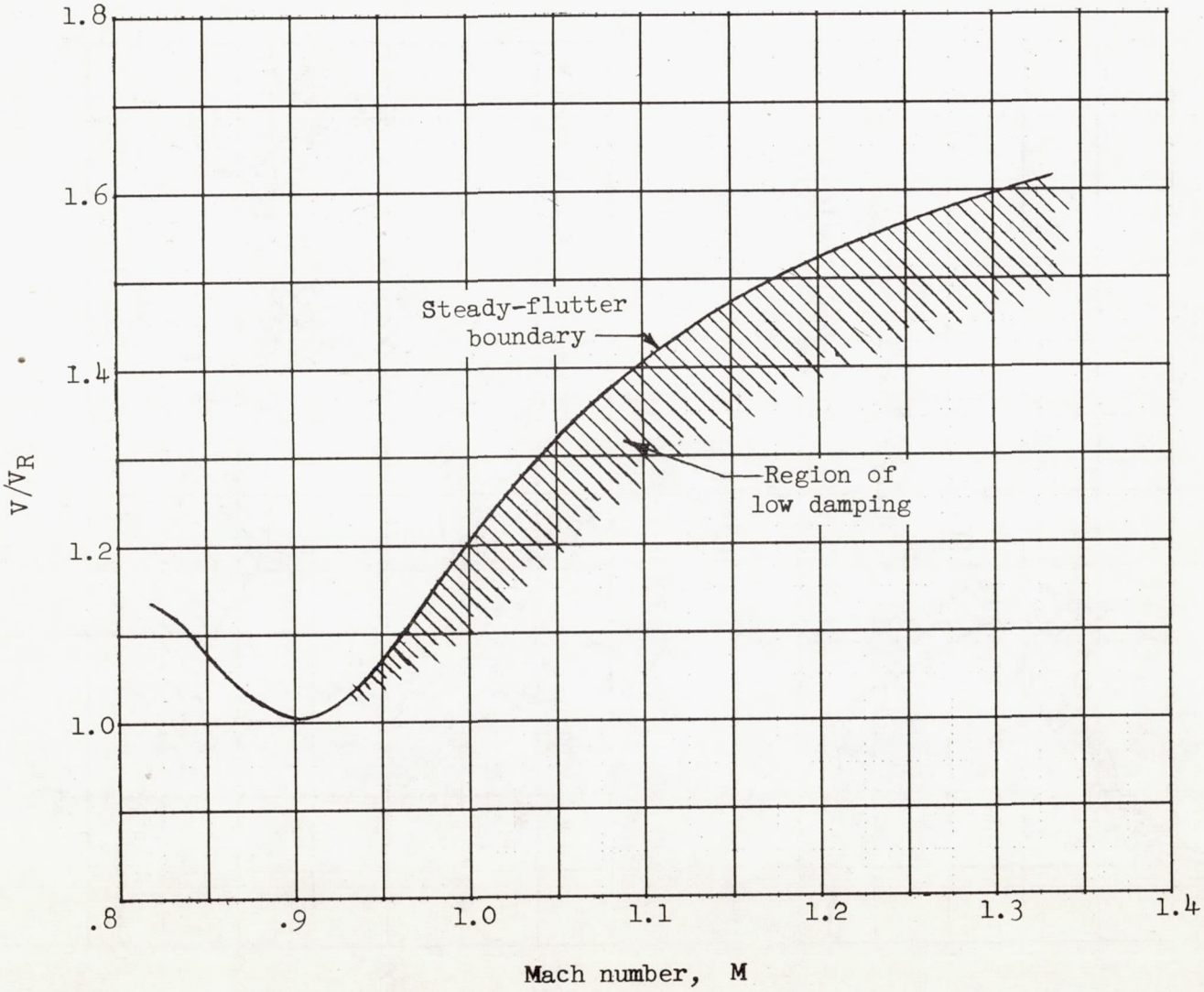

Figure 8.- Effect of Mach number on the extent of the region of low damping.

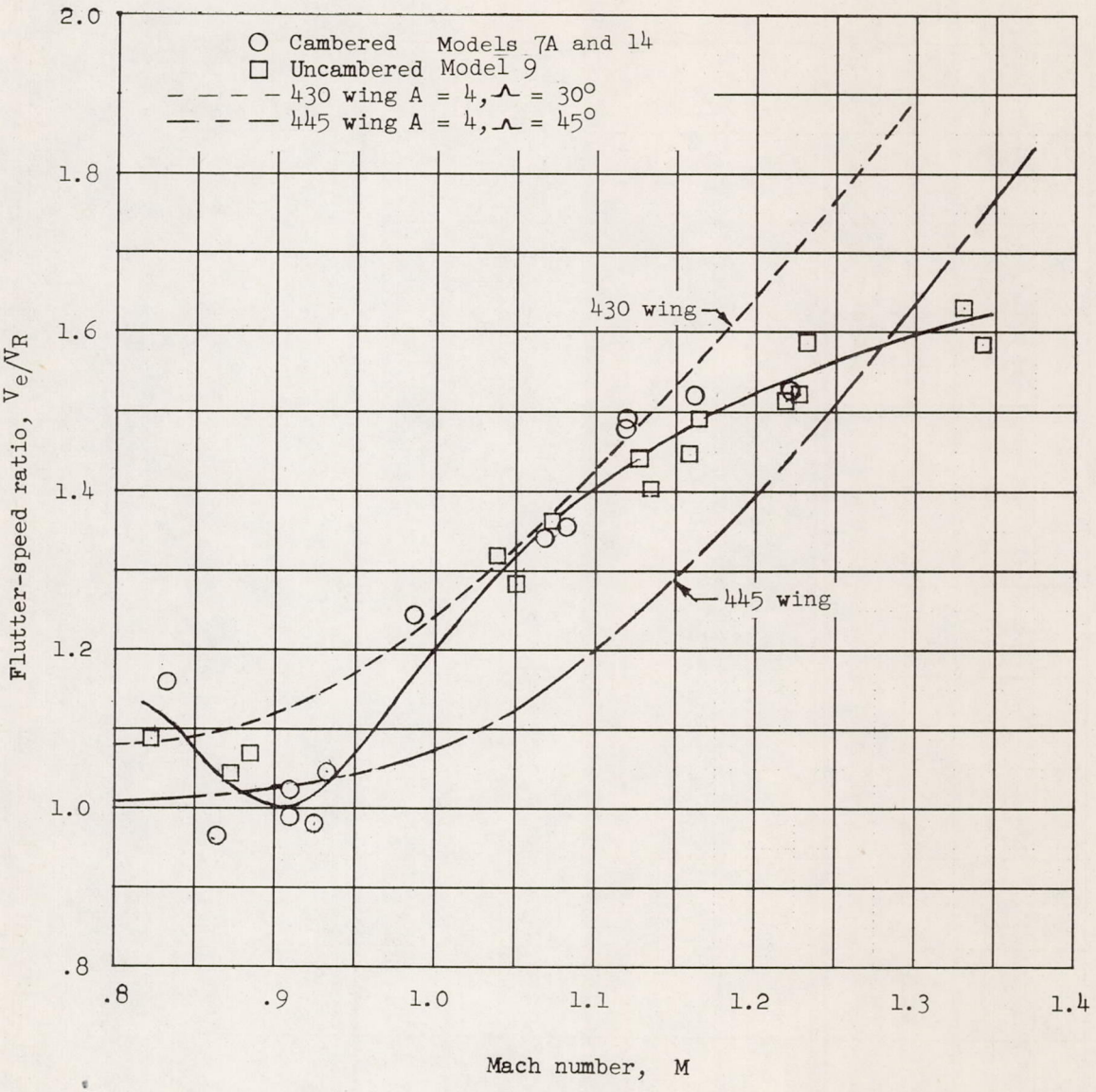

Figure 9.- Effect of Mach number on flutter-speed ratio.